Agricultural and Forest Meteorology 256–257 (2018) 137–149

Contents lists available at ScienceDirect

Agricultural and Forest Meteorology

journal homepage: www.elsevier.com/locate/agrformet

Evaluation of land surface phenology from VIIRS data using time series of PhenoCam imagery

Xiaoyang Zhang[a,b,*], Senthilnath Jayavelu[a], Lingling Liu[a], Mark A. Friedl[c], Geoffrey M. Henebry[a,d], Yan Liu[e], Crystal B. Schaaf[e], Andrew D. Richardson[f,g,h], Joshua Gray[i]

[a] Geospatial Sciences Center of Excellence, South Dakota State University, Brookings, SD 57007, USA
[b] Department of Geography, South Dakota State University, Brookings, SD 57007, USA
[c] Department of Earth and Environment, Boston University, Boston, MA 02215, USA
[d] Department of Natural Resource Management, South Dakota State University, Brookings, SD 57007, USA
[e] School for the Environment, University of Massachusetts Boston, Boston, MA 02125, USA
[f] Department of Organismic and Evolutionary Biology, Harvard University, Cambridge, MA 02138, USA
[g] School of Informatics, Computing, and Cyber Systems, Northern Arizona University, Flagstaff, AZ 86011, USA
[h] Center for Ecosystem Science and Society, Northern Arizona University, Flagstaff, AZ 86011, USA
[i] Department of Forestry and Environmental Resources, North Carolina State University, Raleigh, NC 27695, USA

ARTICLE INFO

Keywords:
Phenocam
VIIRS
Land surface phenology
Validation and evaluation

ABSTRACT

Land surface phenology (LSP) has been widely retrieved from time series of various satellite instruments in order to monitor climate change and ecosystem dynamics. However, any evaluation of the quality of LSP data sets is quite challenging because the in situ observations on a limited number of individual trees, shrubs, or other plants are rarely representative of the landscape sampled in a single satellite pixel. Moreover, vegetation indices detecting biophysical features of vegetation seasonality are different from (but related to) the specific plant life history stages observed by humans at ground level. This study is the first comprehensive evaluation of the LSP product derived from Visible Infrared Imaging Radiometer Suite (VIIRS) data using both MODIS LSP products and observations from the PhenoCam network across the Contiguous United States during 2013 and 2014. PhenoCam observes vegetation canopy over a landscape at very high frequency, providing nearly continuous canopy status and enabling the estimate of discrete phenophase using vegetation indices that are conceptually similar to satellite data. Six phenological dates (greenup onset, mid-greenup phase, maturity onset, senescence onset, mid-senescence phase, and dormancy onset) were retrieved separately from daily VIIRS NDVI (normalized difference vegetative index) and EVI2 (two-band enhanced vegetation index) time series. Similarly, the six phenological dates were also extracted from the 30-min time series of PhenoCam data using GCC (green chromatic coordinate) and VCI (vegetation contrast index) separately. Phenological dates derived from VIIRS NDVI and EVI2 and PhenoCam GCC and VCI were generally comparable for the vegetation greenup phase, but differed considerably for the senescence phase. Although all indices captured green leaf development effectively, performance discrepancies arose due to their ability to track the mixture of senescing leaf colors. PhenoCam GCC and VCI phenological observations were in better agreement with the phenological dates from VIIRS EVI2 than from VIIRS NDVI. Further, the VIIRS EVI2 phenological metrics were more similar to those from PhenoCam VCI than from PhenoCam GCC time series. Overall, the average absolute difference between the VIIRS EVI2 and PhenoCam VCI phenological dates was 7–11 days in the greenup phase and 10–13 days in the senescence phase. The difference was smaller in forests, followed by grasslands and croplands, and then savannas. Finally, the phenological dates derived from VIIRS EVI2 were compared with MODIS detections, which showed a good agreement with an average absolute difference less than a week except for the senescence onset. These results for the first time demonstrate the upper boundary of uncertainty in VIIRS LSP detections and the continuity to MODIS LSP product.

* Corresponding author at: Geospatial Sciences Center of Excellence, South Dakota State University, Brookings, SD 57007, USA.
E-mail address: xiaoyang.zhang@sdstate.edu (X. Zhang).

https://doi.org/10.1016/j.agrformet.2018.03.003
Received 10 November 2017; Received in revised form 21 February 2018; Accepted 4 March 2018
Available online 20 March 2018
0168-1923/ © 2018 Elsevier B.V. All rights reserved.

1. Introduction

Vegetation phenology plays an important role in understanding climate change due to the biophysical nature of the timing of leaf-on and leaf-off (Cleland et al., 2012; Ivits et al., 2012; Menzel et al., 2006; Morisette et al., 2009; Parmesan and Yohe, 2003). Ground-based direct visual observations and measurements have traditionally been used to record the timing of specific phenological events (e.g., flowering) for particular plant species, at small spatial extents (Abu-Asab et al., 2001; Ault et al., 2015; Morin et al., 2009; Richardson et al., 2006; Schwartz et al., 2006, 2013, 2002). Sensors onboard satellite observatories, such as the Advanced Very High Resolution Radiometer (AVHRR) and the MODerate resolution Imaging Spectroradiometer (MODIS), provide Earth observations at nearly global coverage every day. These data allow the seasonal dynamics of the vegetated land surface to be mapped and monitored at regional to global scales. As a result, a variety of land surface phenology (LSP) products have been developed for the study of climate change, ecosystem dynamics, biodiversity, and terrestrial carbon budget at multiple scales (Henebry and de Beurs, 2013). For example, the start and end of vegetation growth, as observed since 1981 at spatial resolutions of 8–16 km, have been extensively investigated using the normalized difference vegetation index (NDVI) data derived from the AVHRR GIMMS (Global Inventory Modeling and Mapping Studies) dataset at local, regional, and global scales (de Beurs and Henebry, 2010; de Jong et al., 2011; Myneni et al., 1997; Reed et al., 1994; White et al., 2009; Zhang et al., 2007). More recently, LSP products with spatial resolutions of 250–1000 m have been produced from MODIS NDVI and enhanced vegetation index (EVI) data, including the USGS EROS 250 m eMODIS LSP data (2001–2014) across the Contiguous United States (CONUS) (cf. Reed et al., 1994); the NASA NACP (North American Carbon Program) 250 m LSP data over North America (Tan et al., 2011); and the NASA 500 m Land Cover Dynamics Products (MCD12Q2) covering the entire globe (Ganguly et al., 2010; Zhang et al., 2006, 2003). Further, for continuity purposes, since the AVHRRs lack a separate blue channel needed to calculate the EVI, the two-band enhanced vegetation index (EVI2; Jiang et al., 2008), which is functionally equivalent to the EVI, has been used to detect long-term global land surface phenology from both AVHHR and MODIS at a spatial resolution of 0.05° (Zhang et al., 2014).

It is challenging to evaluate and validate LSP with in-situ measurements due to vast differences in scale and the different kinds of phenomena being observed. Consequently, the quality of satellite-derived LSP products and their relation to biological events in plants have been poorly characterized. Previous studies evaluated LSP using phenological timing from empirical or bioclimatic models (Schaber and Badeck, 2003; Schwartz, 1999), ground-based cryosphere and hydrology network records (White et al., 2009), phenological measurements from long-term ecological research networks (Ganguly et al., 2010; Soudani et al., 2008; Zhang et al., 2006), gross primary productivity from flux towers (Sakamoto et al., 2010; Xiao et al., 2013), observations of specific species in a phenology network (Delbart et al., 2015; Liang et al., 2014), and landscape phenology indices aggregated from individual plants (Liang et al., 2011). The samples from these assessments are not intrinsically comparable to satellite-derived LSP because different biophysical properties were being measured and the data are available only at very few locations and a limited number of ecosystem types. Thus, these approaches are ineffective for the direct evaluation and validation of LSP data at satellite pixels.

Recently, near-surface remote sensing has been used to provide diurnal monitoring of vegetation developments at canopy to landscape scales without significant impacts from atmospheric scattering or obscuring clouds (Richardson et al., 2009a). The PhenoCam network captures digital images from tower-mounted web cameras, thus providing consistent and continuous monitoring of vegetation canopy conditions at locations throughout the United States (Hufkens et al., 2012; Richardson et al., 2009b, 2007; Sonnentag et al., 2012). The digital repeat photography generated by PhenoCam protocol contains high spatial and temporal resolution imagery composed of red, green, and blue color planes. These images allow for the characterization of seasonal dynamics via image processing approaches similar to those applied to satellite imagery. They also provide the opportunity for visual interpretation of vegetation development, because they appear like ordinary photographs at a familiar resolution. Combining visual interpretation and image processing of PhenoCam time series enables a generalized phenology of the observed vegetation canopies to be characterized. The PhenoCam system and protocols are not able to replace direct high-quality field observations (e.g., date of first leaf, date of flowering, etc.). Thus, time series of PhenoCam observations have been used to monitor vegetation phenology at the local and regional scales (Sonnentag et al., 2012; Toomey et al., 2015). PhenoCam data have also been shown to be a robust tool to evaluate phenological transition dates derived from satellite remote sensing (Keenan and Richardson, 2015; Klosterman et al., 2014; Rodriguez-Galiano et al., 2015).

A well-validated long-term LSP product is critical for investigating the phenological shifts induced by climate change and land disturbance as well as the phenological impacts on ecosystem function, biodiversity, and carbon budgets. For this purpose, MODIS LSP product (MCD12Q2) has been operationally produced in NASA from time series of MODIS observations since 2000 (Ganguly et al., 2010; Zhang et al., 2006, 2003). Because the MODIS sensors are aging and nearing the end of their duty cycles, the Visible Infrared Imaging Radiometer Suite (VIIRS) sensor, onboard the Suomi National Polar-orbiting Partnership (NPP) satellite (launched October 28, 2011), is intended to provide continuity with the MODIS data record (Justice et al., 2013; Roman et al., 2011). During the next few decades, VIIRS on the Joint Polar Satellite System (JPSS) series, which is planned to launch in late 2017 (JPSS-1) and late 2021 (JPSS-2) (Goldberg et al., 2013), will continue to provide the capability to monitor LSP. Thus, the MODIS phenology product (MCD12Q2) will be replaced using LSP retrievals from VIIRS data, which makes it critical now to understand the capabilities of VIIRS observations for LSP detections.

This study is the first comprehensive evaluation of the VIIRS phenology product that will become the operational standard to continue the MODIS phenology record. The three goals of this study are (1) to investigate the differences between NDVI and EVI2 for LSP detections so that the better vegetation index may be selected for VIIRS LSP product generation; (2) to evaluate the accuracy and uncertainty of VIIRS LSP detections by direct comparison against phenological transition dates derived from two indices calculated from PhenoCam data; and (3) to verify that VIIRS will provide continuity with MODIS by directly comparing the VIIRS LSP detections at PhenoCam sites with the corresponding MODIS retrievals.

2. Data and methods

2.1. Land cover and land surface temperature data

To define the land cover types of the VIIRS pixels that the PhenoCams were viewing, we used the International Geosphere-Biosphere Programme (IGBP) scheme in the MODIS land cover product (MCD12Q1) in 2013 (Friedl et al., 2010).

MODIS land surface temperature (LST) product (MOD11A1, V006) at a spatial resolution of 1 km was used from July 2012 to June 2015. The LST data were rescaled to 500 m using a nearest neighbor method to match the spatial resolution of the VIIRS data. These LST time series determined the winter period in the processing of VIIRS time series (cf. Section 2.4). Note that the VIIRS LST product, which is currently under development for operational production by NASA, will eventually replace the MODIS LST after the MODIS sensors reach their end of their duty cycles, by approximately 2021 or sooner.

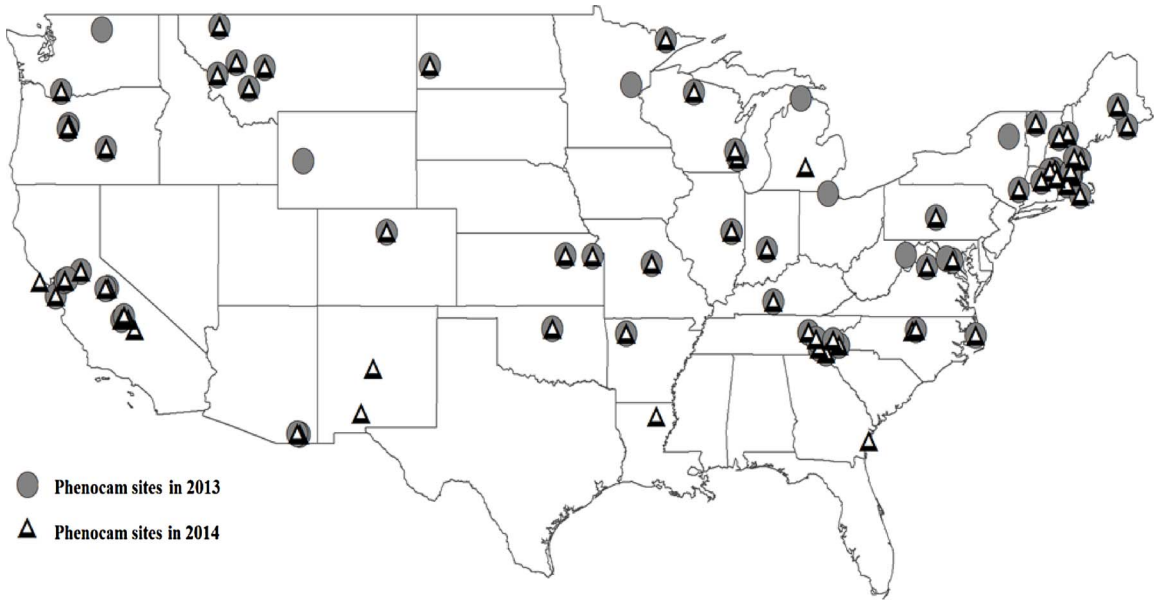

Fig. 1. Spatial distribution of PhenoCam sites in 2013 and 2014.

2.2. PhenoCam data and time series of PhenoCam vegetation indices

The PhenoCam network provides digital photographs every 30 min between 0400 and 2130 local time at most sites. The data are stored on the PhenoCam server (http://klima.sr.unh.edu/) at the University of New Hampshire (Sonnentag et al., 2012). During 2013–2014 there were about 150 sites distributed across North America. After excluding sites without a full year of continuous observations (i.e., some sites were newly established or recorded data temporarily), 82 sites in 2013 and 82 sites in 2014 remained for use in this study (Fig. 1).

PhenoCam digital images are stored in JPEG format, which contain red, green, and blue (RGB) color channels. For this study, RGB data were extracted from polygonal regions of interest (ROI) unique to each site based on the GUI (graphical user interface) tool provided on the PhenoCam project page (https://phenocam.sr.unh.edu/webcam/tools/). Each ROI was constructed to eliminate the influence of non-vegetated areas (e.g., sky, water, bare soil, or rocks) and was selected based on the predominant land cover types in the corresponding VIIRS pixels (Klosterman et al., 2014). In the heterogeneous sites, such as savannas, we selected the ROI containing the most uniform mixture of trees and grasses.

We calculated two vegetation indices for each image using the RGB pixels in each ROI polygon (Fig. 2). The green chromatic coordinate (GCC), which has been frequently used to derive near-surface time series for phenological analysis (Klosterman et al., 2014; Wingate et al., 2015), was calculated from red (R), green (G), and blue (B) digital numbers (DN) in each pixel as follows:

$$GCC = \frac{G}{(R + B + G)} \quad (1)$$

A new related index, the vegetation contrast index (VCI), was calculated in each pixel as follows:

$$VCI = \frac{G}{(R + B)} \quad (2)$$

While GCC describes the proportion of green channel brightness relative to total image brightness, VCI contrasts the green channel relative to the sum of the red and blue channels. The VCI is a nonlinear transform of the GCC resulting in a higher dynamic range for the VCI relative to the GCC.

Across each ROI in each image the GCC and the VCI were averaged separately. Daily time series of GCC and VCI were created from the 30-min values by calculating the 90th percentile of GCC or VCI for each day (Sonnentag et al., 2012). This filtering step minimized the effect of spuriously large and most of low GCC and VCI values arising from image noise and artifacts (Fig. 2). These daily GCC and VCI time series were calculated at each PhenoCam location to detect phenophase transitions (cf. Section 2.4).

2.3. VIIRS NBAR data and VIIRS vegetation indices

The Nadir BRDF (Bidirectional Reflectance Distribution Function)-Adjusted Reflectance (NBAR) data retrieved from daily VIIRS imagery provides the remote sensing data from which to detect land surface phenology. NBAR data are generated by using the daily retrieved BRDF model parameters within a 16-day moving window to correct variations resulting from off-nadir viewing geometry, and to adjust the solar zenith angle to local solar noon (Liu et al., 2017b; Schaaf et al., 2002, 2011; Wang et al., 2012). Thus, the impacts of extreme viewing geometries (± 56° across-track) in the VIIRS surface reflectance data are minimized in the NBAR values. This study generated 14 tiles of 500 m daily VIIRS NBAR data collected between July 1, 2012 and June 30, 2015 (prior to operational production). These tiles (H08V04, H08V05, H08V06, H09V04, H09V05, H09V06, H10V04, H10V05, H10V06, H11V04, H11V05, H12V04, H12V05 and H13V04) covered all of CONUS. The VIIRS NBAR product also provides cloud and snow flags in its quality assurance (QA) data. The QA scores rank from 0 to 3 as follows: QA = 0 indicates “best quality”, where the BRDF model was established using more than 7 cloud-free observations within a 16-day window with a model RMSE (Root Mean Squared Error) of less than 0.08 and a WoD (Weight of Determination) less than 1.65 (indicating an appropriate sampling of the surface anisotropy); QA = 1 indicates “other quality”, where the RMSE and WoD of the BRDF model were larger but still acceptable; QA = 2 or 3 both indicate “poorer quality”, where cloud-free observations were only available from 2 to 7 days or magnitude inversion was used; and QA = 4 indicates “fill value”, where cloud-free observations were less than 2 days (Liu et al., 2017b). Finally, snow retrieval was applied when snow reflectance observations were used (Liu et al., 2017b).

Although many vegetation indices have been used to analyze vegetation dynamics (Huete et al., 2013; Vina et al., 2012), the NDVI has been most widely used to investigate local and global vegetation properties, including phenology, land cover type, net primary production, and aboveground biomass (Carlson and Ripley, 1997; Friedl et al.,

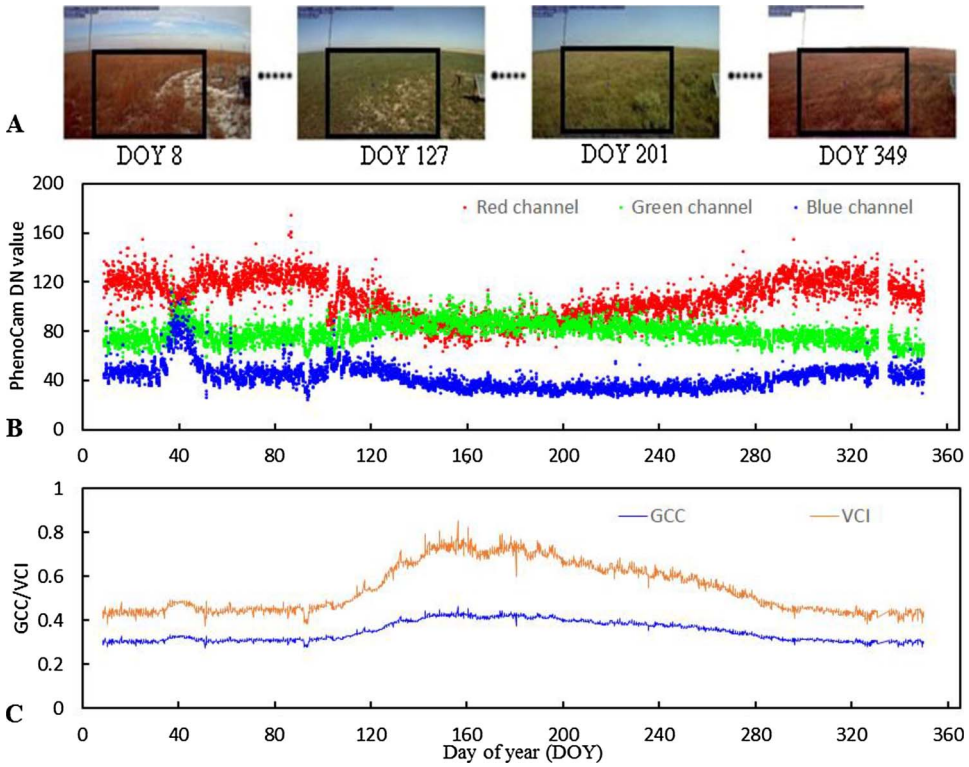

Fig. 2. Variations of PhenoCam observations in the Konza Prairie Biological Station, Kansas State University, Kansas. (A) Extracted ROI from imagery, (B) RGB DN values averaged from ROI in a 30-min interval, (C) diurnal variation (every 30 min) in GCC and VCI.

2002; Myneni et al., 2002; White et al., 1997). Relative to the NDVI, the enhanced vegetation index (EVI) (Huete et al., 2002) is less sensitive to bare ground cover and atmospheric effects and retains a higher sensitivity over denser vegetation canopies than the NDVI (Huete et al., 2002). Calculation of EVI requires reflectance values in the near-infrared, red, and blue wavelengths, but some coarse-spatial resolution spectroradiometers (e.g., AVHRR and 500 VIIRS NBAR) lack blue channels. To overcome this limitation, an alternative two-band EVI (EVI2) was developed using the relationship between red and blue bands (Huete et al., 2006; Jiang et al., 2008):

$$EVI2 = G\left(\frac{\rho_{NIR} - \rho_{red}}{\rho_{NIR} + \rho_{red} + L}\right) \quad (3)$$

where ρ_{NIR} and ρ_{RED} are spectral reflectances acquired in the near-infrared and red regions, L is the canopy background adjustment (equal to 1), C is aerosol resistance coefficient (equal to 2.4), and G is a gain factor with a value of 2.5.

Here, daily VIIRS NDVI and EVI2 values were derived from the VIIRS NBAR spectral reflectance data of red band (I1: 0.640 μm) and near infrared band (I2: 0.865 μm) to detect phenophase transition dates over CONUS in 2013 and 2014.

2.4. Land surface phenology detections from time series data

Many methods have been developed to reduce noise, enhance signal, and retrieve land surface phenology from time series of vegetation indices. These methods include a Fourier harmonic function (Moody and Johnson, 2001), a Gaussian function (Jonsson and Eklundh, 2002), a piecewise-logistic function (Zhang et al., 2003), Adaptive Savitzky–Golay filter (Chen et al., 2004), a convex quadratic function based on accumulated growing degree-days (de Beurs and Henebry, 2004; Henebry and de Beurs, 2013), a polynomial curve function (Bradley et al., 2007), iterative "Caterpillar" singular spectrum analysis method (Golyandina and Osipov, 2007), temporal smoothing and gap filling (Verger et al., 2011), and consistent adjustment of the climatology to actual observations (Verger et al., 2013). Due to the complexity of satellite sensor time series, each method has its distinct advantages and disadvantages, which have been shown in various intercomparisons (Atkinson et al., 2012; Hird and McDermid, 2009; Kandasamy et al., 2013; Kandasamy and Fernandes, 2015; White et al., 2009).

Here we used the Hybrid Piecewise Logistic Model (HPLM) based Land Surface Phenology Detection (LSPD) algorithm (HPLM-LSPD) (Zhang, 2015; Zhang et al., 2003). The HPLM-LSPD algorithm offers several advantages: each model parameter can be assigned to a biophysical meaning related to vegetation growth or senescence; the model is capable of flexibly describing either symmetric or asymmetric development of vegetation indices with multiple cycles of vegetation growth; and phenophase transition dates are determined from the fitted parameter coefficients rather than from predefined thresholds.

The followings provide a brief description of HPLM-LSPD algorithm for retrieving phenological transition dates from daily PhenoCam time series of GCC and VCI and, separately, from the daily VIIRS NBAR time series of NDVI and EVI2. The daily VIIRS NBAR vegetation indices (VI) were aggregated into separate 3-day composites by first selecting the highest quality data (cloud-free observations) and then selecting the maximum value if more than one VI value within the 3-day period had the same quality. VIs contaminated by snow were replaced using background observations at each site; this background value was determined using the mean of the top 50 percentile of cloud and snow-free winter VI values (denoted using VIIRS NBAR QA flag) during the winter period when LST ≤ 278 K (Zhang, 2015). Data gaps in the time series caused by poor quality observations (fill values defined in the VIIRS NABR QA) were replaced using a moving average of neighboring good quality data. Finally, a Savitzky–Golay filter was used to smooth the VI time series.

The HPLM approach was used to fit time series of PhenoCam GCC and VCI and VIIRS NDVI and EVI2, separately, at each PhenoCam location. The logistic model in HPLM is a physically-based model

developed for monitoring crop growth (Richards, 1959; Ratkowsky, 1983) and has been adopted to simulate the temporal trajectory of the development of canopy "greenness" (Zhang et al., 2003). Apparent greenness could decrease slightly under summer water stress or other impacts, which would result in a greenness trajectory differing from that occurring under optimally favorable weather conditions. The greenness under stress can be described by adding an impact factor to the logistic model (Elmore et al., 2012; Melaas et al., 2013). To simulate vegetation greenness trajectories effectively, the HPLM was characterized based on the following functions (Zhang, 2015):where VI is vegetation index, t is time in the day of year (DOY), a is related to the vegetation growth time, b is associated with the rate of plant leaf development, c is the amplitude of VI variation, d represents vegetation under summer water stress or other impacts, and VI_b is the background VI value. In order to determine whether the vegetation suffers from stress or not, Eqs. (4) and (5) were compared in fitting the temporal VI time series and the function with better fit was chosen (Zhang, 2015).

In the fitted HPLM, the extreme points in the curvature change rate of the reconstructed temporal trajectories indicate the phenophase transition dates (Zhang et al., 2006, 2003). Specifically, the curvature (K) for the HPLM models was calculated as follows:

$$K(t) = \frac{d\alpha}{ds} = \frac{VI(t)''}{(1 + VI(t)'^2)^{\frac{3}{2}}} \quad (6)$$

where α is the angle in radians of the unit tangent vector at time t along a differential curve, s is the unit length of the curve, VI(t) is calculated from Eqs. (4) or (5), and ′ and ″ denote the first and second derivatives, respectively.

The curvature change rate (K'), which is the first derivative of the curvature K for the HPLM (Eq. (6)), determined the four key phenological transition dates (Zhang et al., 2006, 2003). During the vegetation greenup phase, three extreme points were identified from the VI curvature change rate (K'). The two maximum values correspond to the greenup onset [i.e. start-of-spring (SOS)] and maturity onset [i.e. end-of-spring (EOS)], respectively. Transition dates of both senescence onset [i.e. start-of-fall (SOF)] and dormancy onset [i.e. end-of-fall (EOF)] during a senescence phase were estimated in a similar fashion. These four key transition dates characterize the start of four generalized vegetation growth phases: greenup, maturity, senescence, and dormancy. We also determined the mid-greenup phase [i.e. middle-of-spring (MOS)] and mid-senescence phase [i.e. middle-of-fall (MOF)] at 50% of the seasonal amplitude. The latter two metrics could be used to characterize the phenological timings within greenup and senescence phase, such as 4 or 5 nodes for soybean and 8 or 9 leaves for corn during crop greenup, and near-peak coloration of deciduous forests during senescence phase (Zhang et al., 2012). Moreover, these two metrics are often used to define vegetation growing season from satellite data in various studies (White et al., 2009; White and Nemani, 2006; White et al., 1997). Thus, this study focuses on a total of six phenological dates (Fig. 3). Phenophase transition dates detected from VIIRS NDVI or EVI2 time series are hereafter referred to as "VIIRS phenology" and, likewise, those detected from GCC or VCI time series as "PhenoCam phenology".

The quality of the VIIRS time series data significantly impacts the confidence of vegetation phenology detection (Zhang, 2015; Zhang et al., 2017). Specifically, seasonal dynamics in the VIIRS NDVI and EVI2 may not be properly reconstructed if cloud cover or other sources cause long gaps in the time series. Thus, phenology detection quality was evaluated using the local proportion of high quality observations available during each three 3-day period before and after each of the four retrieved phenophase transitions, separately (Zhang et al., 2017): greenup onset, maturity onset, senescence onset, and dormancy onset. It requires at least one high quality (best quality or other quality. cf. Section 2.3) observation that is available within an 8-day period to derive reliable phenophase transition dates (Zhang et al., 2009b). The retrieval of a phenological event was considered as "high confidence" only if the corresponding local proportion of good quality VIIRS observations was larger than 60%. Otherwise, it was flagged as "low confidence".

2.5. Evaluation of VIIRS phenology using PhenoCam phenology

We first compared the statistical relationships among the time series of NDVI, EVI2, GCC, and VCI. This comparison provided us the similarity of different vegetation indices in tracing temporal development of the vegetated land surface.

Phenological metrics from VIIRS NDVI and EVI2 time series were further evaluated using phenophase transition dates retrieved from PhenoCam GCC and VCI. Average absolute difference (AAD), bias, and coefficient of determination (R^2) from linear regression models were used to quantify agreement between the VIIRS and PhenoCam phenophase transitions. AAD is a measure of statistical dispersion equal to the average absolute difference of two independent variables (VIIRS phenology and PhenoCam phenology). Bias quantifies the average overestimation (positive bias) or underestimation (negative bias). A reduced major axis regression was used to examine the correlations between samples of PhenoCam and VIIRS phenophase transition dates because this regression accounts for uncertainty in both the dependent and independent variables.

Each of these statistical parameters was estimated for each of the six phenophase transition dates derived from the VIIRS data and PhenoCam imagery (164 site-years during 2013 and 2014). We also stratified the phenological dates based on IGBP land cover type (cf. Section 2.1). In particular, we focused on forests (mixed forests and deciduous broadleaf forests), croplands, grasslands, and savannas (woody savannas and savannas), which accounted for 53%, 11%, 10%, and 10% of PhenoCam sites, respectively. Other land cover types were not investigated because they had low representation in the PhenoCam sites available for statistical analysis.

2.6. Comparison of VIIRS phenology with MODIS phenology

VIIRS phenology was compared with MODIS phenology at selected PhenoCam locations to investigate the data product continuity between the two sensors. Therefore, we also collected the Collection V006 daily gridded 500m MODIS NBAR data from the MODIS operational BRDF, Albedo and NBAR products (MCD43) (Schaaf et al., 2002, 2011; Wang et al., 2012). MODIS NBAR is produced based on multiple observations from the MODIS sensors on both the Terra and Aqua satellite platforms. The MODIS phenology detections were conducted using the algorithm described in Section 2.4. Finally, six phenological transition dates from VIIRS EVI2 at the Phenocam sites were compared with those from MODIS EVI2, separately, by calculating the reduced major axis regression and the average absolute difference.

3. Results

3.1. Trajectories of PhenoCam and VIIRS data and retrieved phenophase transition dates

Fig. 2 shows data from PhenoCam observations over grasslands at the Konza Prairie Biological Station, near Manhattan, Kansas, USA, to illustrate the nature and quality of phenological information that is available from PhenoCam imagery. While the diurnal RGB DN values fluctuated greatly with only modest seasonality (Fig. 2B), the calculated GCC and VCI substantially reduced the fluctuations (Fig. 2C).

Fig. 3 presents the six phenophase transition dates retrieved from the VIIRS and PhenoCam time series at the Konza Prairie Biological Station during 2014. Visual inspection of the PhenoCam images verified similar temporal developments of the NDVI, EVI2, GCC, and VCI time series. Specifically, SOS was clearly related to the timing of leaf emergence, and EOS corresponded to timing approaching maximum green

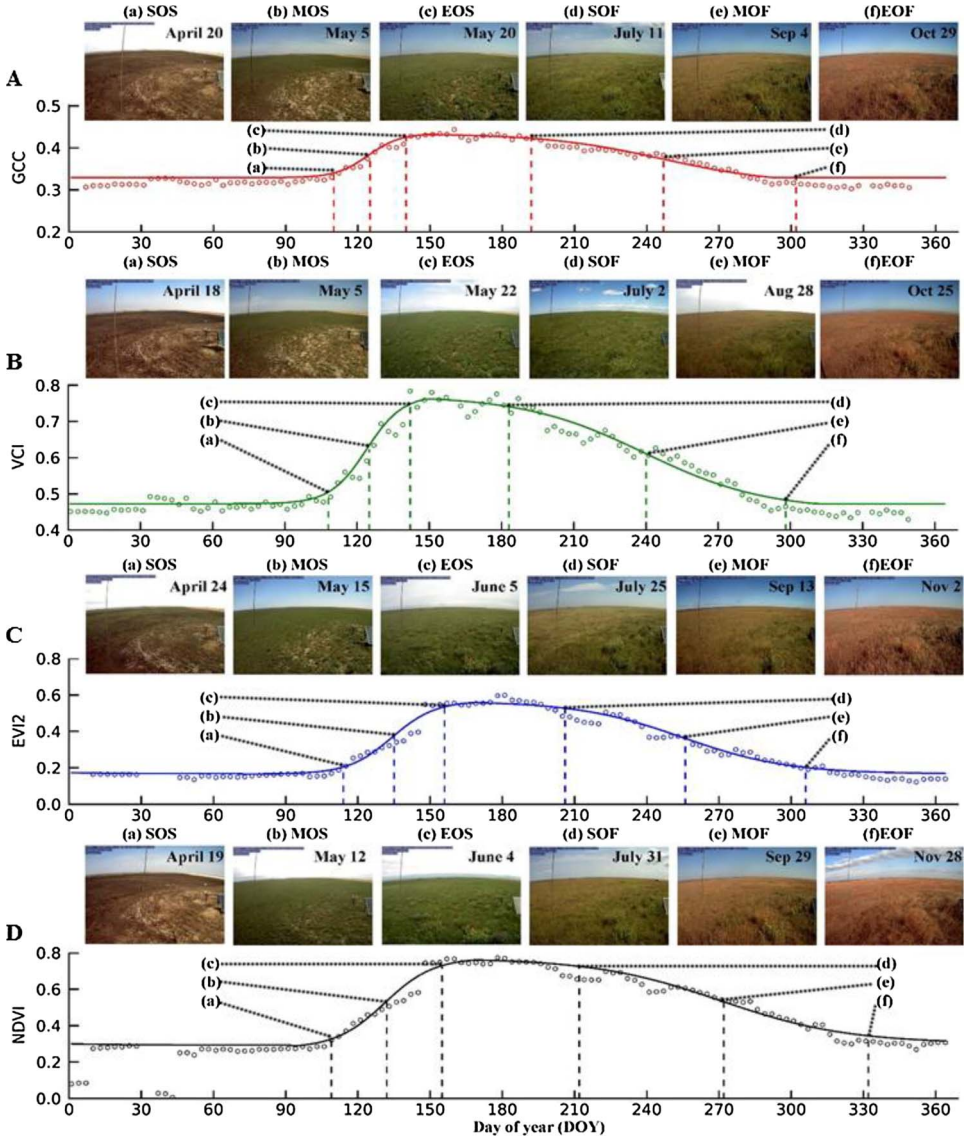

Fig. 3. Temporal variations in PhenoCam observations and phenology detections from GCC (A), VCI (B), EVI2 (C), and NDVI (D) in the Konza Prairie Biological Station, Kansas State University, Kansas. The dots are raw observations and the solid lines are fitted curves. The symbols of a, b, c, d, e and f represent the phenological timings of SOS, MOS, EOS, SOF, MOF, and EOF with corresponding images, respectively.

grass cover. Similarly, SOF was associated with the start of leaf senescence and EOF corresponded to widespread brown grasses. At Konza, the six phenophase transition dates (SOS, MOS, EOS, SOF, MOF, EOF) derived from each time series were comparable. In particular, the SOS difference was less than 6 days from all vegetation indices, and their EOF difference was less than 8 days, except for the NDVI. However, the difference in EOS and SOF between VIIRS and PhenoCam phenology detections was relatively large.

3.2. Phenophase transition dates from PhenoCam indices

Phenological metrics from PhenoCam GCC and VCI data were in very close agreement for all six phenophase transition dates (Table 1 and Fig. 4). Phenological differences were relatively smaller for spring greenup than senescence; specifically, the AAD was less than 2 days in spring but more than 3 days in autumn. The largest differences were associated with the timing of senescence onset. Analysis of bias statistics indicates that the spring phenological dates from GCC were slightly earlier than those from VCI, while the pattern was reversed during autumn senescence phenology (Table 1). Results from regression models show that the slope between dates retrieved from GCC and VCI was close to 1 and coefficients of determination (R^2) were over 0.94, although R^2 values were slightly higher during spring than in autumn.

3.3. Comparison of phenophase transition dates from VIIRS indices

Phenological detections from the VIIRS NDVI and EVI2 time series were compared at each PhenoCam site in 2013 and 2014 (Table 1, Fig. 5). AADs from spring greenup were less than 7 days, which was much less than the AADs of 12–19 days found during autumn senescence. The smallest difference appeared in MOS, while the largest difference appeared in SOF. Bias statistics show there were no systematic differences between NDVI and EVI2 detections in the spring phenological dates; however, EVI2-based retrievals were 6–17 days earlier than NDVI-based retrievals for the phenological events of senescence in autumn (Table 1). Regression models indicated that slopes were closer to unity and the intercepts were smaller in the greenup phase than in the senescence phase (Fig. 5). The coefficients of determination were all highly significant, and larger than 0.9 in the spring phases, but somewhat lower for the autumn phases ($R^2 \geq 0.72$).

Excluding low confidence retrievals (local good quality observation < 60%), decreased slightly the differences in phenophase

Table 1
Statistical comparison of phenological transition dates estimated from PhenoCam GCC and VCI and VIIRS NDVI and EVI2 in PhenoCam sites. Units for Average Absolute Difference (AAD) and Bias are days. AAD values are mean and one standard deviation. Positive (negative) bias means GCC or NDVI dates are later (earlier) than VCI or EVI2 dates.

Vegetation index	Statistic parameters	Greenup phase			Senescence phase		
		SOS	MOS	EOS	SOF	MOF	EOF
GCC vs. VCI	AAD	1.9 ± 3.9	1.1 ± 2.1	1.3 ± 2.6	5.1 ± 7.5	3.8 ± 6.3	3.7 ± 6.1
	Bias	−2	−1	0	1	3	2
	R^2	0.98	0.99	0.98	0.94	0.97	0.97
NDVI vs. EVI2	AAD	5.9 ± 7.7	4.8 ± 6.1	6.5 ± 6.8	19.2 ± 10.8	15.3 ± 8.9	11.6 ± 10.4
	Bias	1	0	0	17	13	6
	R^2	0.91	0.93	0.91	0.89	0.89	0.72
NDVI vs. EVI2 (excluding sites with low confidence)	AAD	4.7 ± 4.7	4.3 ± 4.9	6.1 ± 6.2	18.4 ± 10.1	14.6 ± 7.9	10.5 ± 9.1
	Bias	1	0	−1	17	12	5
	R^2	0.95	0.95	0.92	0.90	0.91	0.78

transition dates between NDVI and EVI2: AAD decreased by 0.5–1 days (Table 1). As expected, VIIRS data quality affects the detection of phenological dates in NDVI and EVI2 time series.

3.4. Comparison of VIIRS phenology with PhenoCam phenology

The statistical relationship among EVI2, NDVI, VCI, and GCC time series reflects similarity in tracing the vegetation phenology development. Specifically, PhenoCam VCI values exhibit significant positive correlation with both VIIRS EVI2 and NDVI across all the sites with coefficients of determination (R^2) of 0.919 ± 0.059 (ranging from 0.739 to 0.998) and 0.837 ± 0.098 (ranging from 0.585 to 0.982), respectively. The comparison of the mean correlation coefficient between EVI2 and VCI with that between NDVI and VCI shows a Z-score of 4.14 (p-value < 0.0001). Similarly, PhenoCam GCC is significantly correlated to VIIRS EVI2 and NDVI with R^2 of 0.906 ± 0.097 (ranging from 0.389 to 0.999) and 0.839 ± 0.106 (ranging from 0.405 to 0.978), respectively. The comparison of the mean correlation coefficient between EVI2 and GCC with that between NDVI and GCC shows a Z-score of 3.34 (p-value < 0.001). These correlations and Z-scores suggest that the relationship between VIIRS EVI2 and PhenoCam VCI is stronger and VIIRS EVI2 is superior to VIIRS NDVI in capturing temporal PhenoCam VCI and GCC variations.

Table 2 presents statistical comparisons of the phenophase transition dates from the VIIRS NDVI and EVI2 time series (excluding low confidence retrievals) with the PhenoCam GCC and VCI data. For each phenological event, smaller AADs occurred between VCI and EVI2 detections. In contrast, larger AADs occurred between retrievals from GCC and NDVI in spring and between the VCI and NDVI retrievals in autumn, except for EOF. Overall the AADs were much smaller during spring than autumn. The differences increased slightly from the SOS to the EOS during the greenup phase while the differences decreased from the SOF to EOF for the senescence phase. Moreover, both VIIRS (NDVI and EVI2) retrievals in spring were more comparable with PhenoCam VCI than GCC phenology, while the pattern of difference between VIIRS and PhenoCam phenological dates was mixed in autumn. Because of the similarity between GCC and VCI phenology, we focus hereafter on VCI PhenoCam phenology results. Bias shows that the PhenoCam phenology was generally earlier than the VIIRS phenology, except for the critical SOS event where the bias was less than 1 day. Regression models between VIIRS phenology and PhenoCam phenology indicated strong correspondence ($R^2 \geq 0.78$) with slopes close to 1 (Fig. 6).

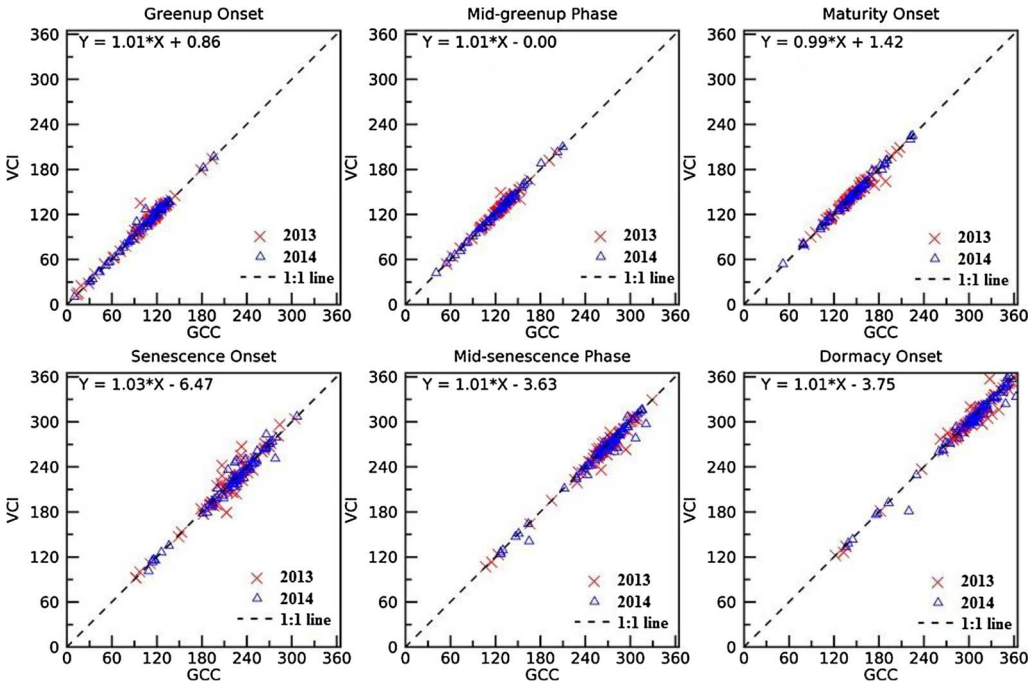

Fig. 4. Comparison of phenology transition dates (DOY) between PhenoCam GCC and VCI estimates in 2013 and 2014.

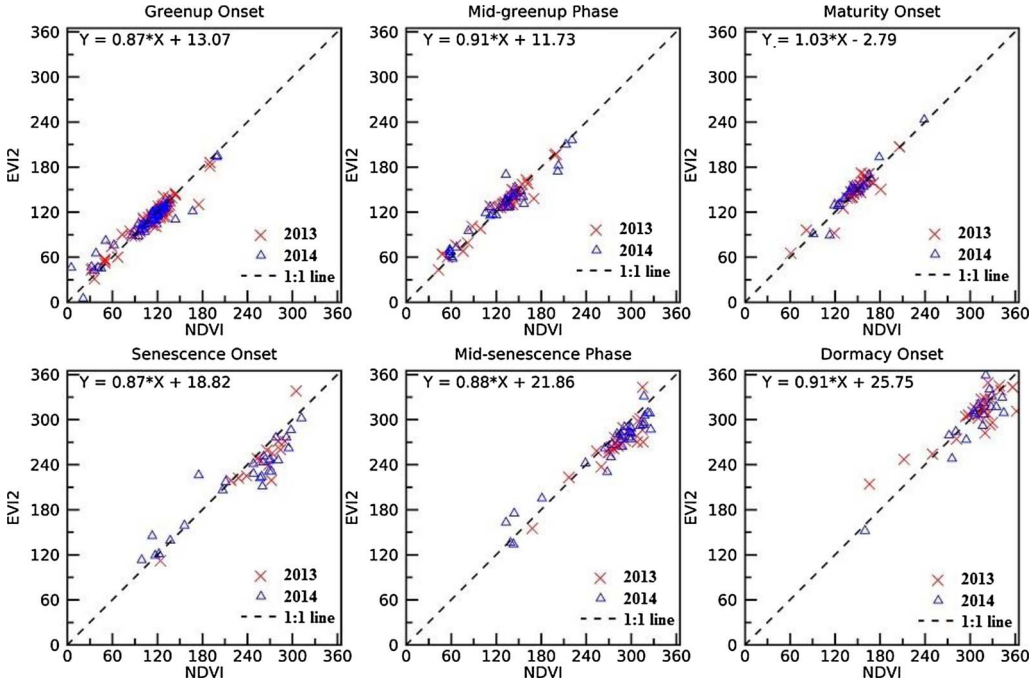

Fig. 5. Comparison of phenology transition dates (DOY) between VIIRS NDVI and EVI2 estimates in 2013 and 2014.

Table 2
Statistical comparison of phenological transition dates estimated from VIIRS NDVI and EVI2 (excluding low quality time series) with those from PhenoCam GCC and VCI in PhenoCam sites. Units for Average Absolute Difference (AAD) and Bias are days. AAD values are mean and one standard deviation. Positive (negative) bias means PhenoCam dates are later (earlier) than VIIRS dates.

PhenoCam index	Remote index	Statistic	Greenup phase			Senescence phase		
			SOS	MOS	EOS	SOF	MOF	EOF
GCC	NDVI	AAD	8.0 ± 6.5	8.6 ± 5.3	11.4 ± 6.8	22.8 ± 12.2	19.2 ± 11.8	16.5 ± 12.2
		Bias	−2	−5	−6	−15	−14	−5
		R^2	0.87	0.88	0.79	0.79	0.80	0.79
	EVI2	AAD	7.4 ± 6.2	8.3 ± 5.1	11.1 ± 6.9	13.3 ± 9.4	11.2 ± 8.2	10.2 ± 7.1
		Bias	0	−5	−7	−3	−3	−3
		R^2	0.87	0.88	0.81	0.79	0.80	0.78
VCI	NDVI	AAD	7.3 ± 5.8	8.3 ± 5.9	11.1 ± 6.5	23.3 ± 13.2	20.4 ± 12.9	16.1 ± 12.5
		Bias	0	−4	−6	−18	−17	−6
		R^2	0.89	0.87	0.81	0.80	0.80	0.79
	EVI2	AAD	6.9 ± 5.8	7.7 ± 5.1	11.0 ± 6.8	13.0 ± 8.5	11.4 ± 8.1	10.0 ± 7.0
		Bias	1	−4	−7	−2	−5	−3
		R^2	0.89	0.88	0.81	0.81	0.81	0.78

3.5. Differences between the PhenoCam and VIIRS phenophase transition dates across different land cover types

Fig. 7 presents a comparison of VCI and EVI2 time series for selected sites with contrasting land covers. As expected, raw EVI2 time series derived from a single VIIRS pixel could be relatively noisy and include large gaps, leading to inaccurate detection of phenological dates. In contrast, the near-surface VCI observations appeared minimally impacted by atmospheric effects exhibiting more stable phenological curves. Visual inspection showed strong correspondence between the EVI2 and VCI seasonal trajectories during 2013 and 2014. Additionally, the HPLM-simulated curves generally do a good job of reproducing the seasonal dynamics in both EVI2 and VCI for all four sites, although the modeled curves smooth out some of the rapid dynamics evident in the VCI time series. However, seasonal trajectories show distinct differences among different land cover types. In the forest site (Harvard Barn), VCI increased faster than EVI2 in the spring greenup phase but they decreased in a similar pattern during the senescence phase. In cropland site (Uiefmaize), VCI could decrease rapidly relative to EVI2. The temporal pattern between EVI2 and VCI could differ in difference growing phases in grassland (Lethbridge) and savanna (Monture) sites. The temporal pattern also shows that the similarity between EVI2 and VCI could vary interannually. Moreover, the amplitude EVI2 or VCI during the growing season indicates that the seasonality in forest and crop sites was stronger than in grass and savanna sites (Fig. 7).

Table 3 presents a summary of the comparisons between phenophase transition dates from VIIRS EVI2 and those from PhenoCam VCI for different land cover types, revealing ecosystem-dependent differences. Several patterns are evident in the results (Table 3). First, detection of spring phases is better in forests than in croplands or grasslands than in savannas. Second, detection of spring phases are better than analogous autumn phases. Third, biases in land cover types featuring woody vegetation (forests and savannas) was lower in absolute terms across spring and autumn phases than croplands and grasslands, where herbaceous vegetation dominates. Fourth, herbaceous cover types exhibited strong negative biases at end of season with VCI dates being 6–17 days earlier than EVI2 dates. Fifth, PhenoCam spring green up dates are later than EVI2 dates for croplands and grasslands. Sixth,

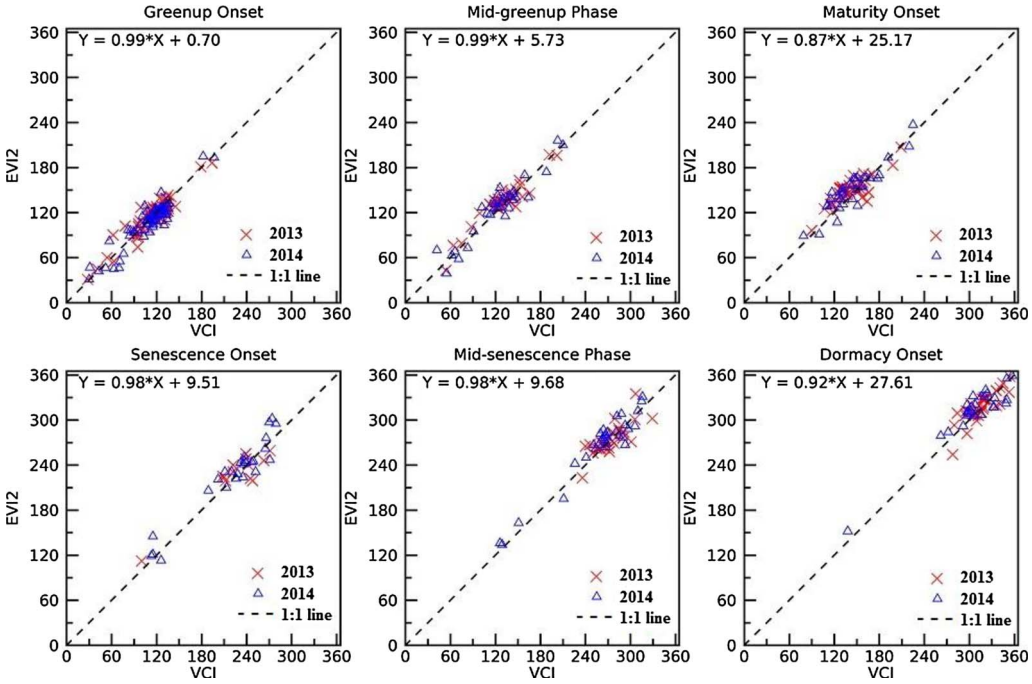

Fig. 6. Comparison of phenology transition dates (DOY) between PhenoCam VCI and VIIRS EVI2 estimates in 2013 and 2014.

coefficients of determination are generally lower (poorer fits) for autumn than spring phases.

In forests, AAD was as low as 6 days for the SOS and as large as 9 days for the EOS. Systematic bias was largest for the EOS, followed by the MOS. These results suggest that all phenological events were realistically detected with similar uncertainties, with typical differences of less than 6 days when the effect of systematic bias was removed.

AAD value between VCI and EVI2 phenologies in croplands varied between 9 and 13 days for all phenophase transitions except SOF. The SOF difference in the AAD was as large as 18 days. Similar differences

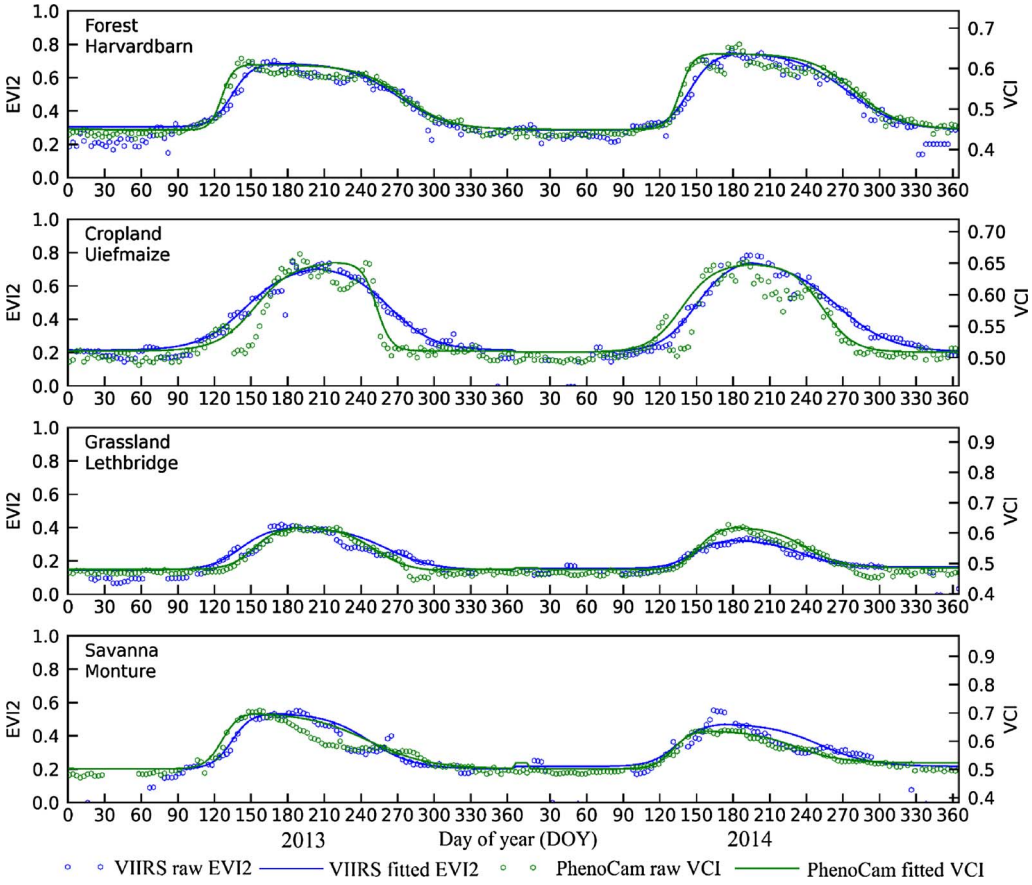

Fig. 7. Comparison of temporal variations in PhenoCam VCI and VIIRS EVI2 in different land cover types.

Table 3
Comparison of phenological transition dates between VCI and EVI2 detections in different land cover types. Units for Average Absolute Difference (AAD) and Bias are days. AAD values are mean and one standard deviation. Positive (negative) bias means VCI dates are later (earlier) than EVI2 dates.

Land cover type	Statistic	Greenup phase			Senescence phase		
		SOS	MOS	EOS	SOF	MOF	EOF
Forest	AAD	5.8 ± 5.1	6.9 ± 4.2	9.2 ± 5.3	6.6 ± 4.5	6.3 ± 4.4	7.4 ± 4.8
	Bias	0	−6	−8	−1	−2	−2
	R^2	0.87	0.79	0.76	0.64	0.69	0.76
Cropland	AAD	9.4 ± 9.5	9.3 ± 5.6	12.7 ± 5.2	18.0 ± 10.6	11.8 ± 9.4	11.2 ± 7.6
	Bias	5	−3	−9	4	−6	−10
	R^2	0.83	0.87	0.69	0.77	0.56	0.69
Grassland	AAD	9.1 ± 6.4	10.1 ± 7.3	10.6 ± 8.8	11.2 ± 7.4	13.7 ± 4.8	17.0 ± 12.0
	Bias	6	1	4	−2	−10	−17
	R^2	0.89	0.87	0.81	0.52	0.62	0.64
Savannas	AAD	12.2 ± 9.6	11.4 ± 8.2	13.0 ± 12.8	24.4 ± 18.8	23.9 ± 17.8	29.2 ± 24.2
	Bias	0	−2	−1	−1	0	−4
	R^2	0.80	0.84	0.80	0.79	0.86	0.78

occurred in the grasslands, where the largest AAD value was found for the EOF. Bias indicated that the VCI phenophase transition dates were earlier than the EVI2 detections in some events but later in others.

AAD value in savannas was the largest among all the land cover classes. AAD was 11–13 days for the spring phenological dates, but 24–29 days for the senescence events (Table 3). Bias was relatively small, suggesting that the differences were mainly associated with random variations.

3.6. Continuity of phenology detections from MODIS to VIIRS

Fig. 8 compares VIIRS phenology detection dates with those from MODIS. The timings of the phenophase transitions exhibited highly significant positive correlation with coefficients of determination ranging from a low of 0.88 for senescence onset to a high of 0.96 for dormancy onset. Smaller AADs appeared for the mid-season dates in both spring and autumn. The largest discrepancy (~9 days) appeared in the senescence onset date in contrast to the greenup onset date discrepancy of ~6.5 days. With the exception of the onset of senescence the AADs were less than a week.

4. Discussion and conclusion

This study comparing phenophase transition dates retrieved from near-surface PhenoCam and satellite-based VIIRS vegetation indices offers several new approaches and important findings. First, our analysis is the first to evaluate comprehensively the phenology products derived from VIIRS, which exemplifies the operational spectroradiometers following the MODIS era. The MODIS data record will end in approximately 2021 or sooner, while the VIIRS on JPSS series will remain operational through the next few decades.

Second, compared to previous evaluations of MODIS phenology products using PhenoCam data (Hufkens et al., 2012; Klosterman et al., 2014), we used here a much larger evaluation data set, consisting of 164 PhenoCam sites across multiple cover types. Third, we introduce the VCI, a new PhenoCam index related to the widely-used GCC, but which offers increased dynamic range. Fourth, our results show generally strong agreement between EVI2 from VIIRS and VCI from

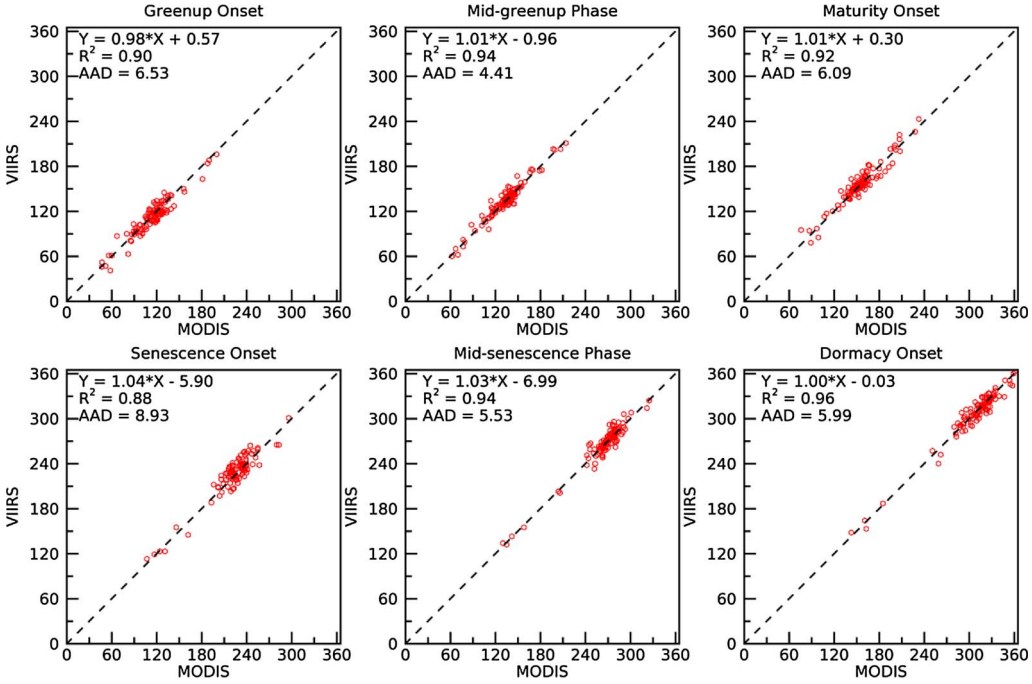

Fig. 8. Comparison of six phenological dates detected from MODIS and VIIRS time series over the PhenoCam sites in 2013 and 2014.

PhenoCam. Fifth and perhaps most critical, our results demonstrate tight linkages between VIIRS and MODIS phenology detections ($R^2 \geq 0.9$ and AAD < 7 days for five out of the six phenological dates) giving us high confidence both in the VIIRS phenological retrievals and in the ability of VIIRS to provide continuity with the MODIS record.

Time series of the vegetation indices were modeled using the physically-based HPLM-LSPD, which provided the functional descriptions of vegetation dynamics from which phenophase transitions were retrieved. HPLM-LSPD captures the four phenological phases (greenup phase, maturity phase, senescence phase, and dormancy phase) in a vegetation growing cycle with four key phenophase transition dates and two additional middle of phase values (middle of the greenup phase and the senescence phase separately). Although PhenoCam time series might be better fitted using more complex and generalized sigmoidal models (Klosterman et al., 2014), more sophisticated models are also sensitive to over-fitting to small variations associated with noise or short frequency transient greenness variations. Moreover, the phenological dates in this study were identified using the change of curvature rate, a strategy that can detect phenological variations from various curves with or without distinctive vegetation seasonality.

Phenophase transition dates derived from both PhenoCam and VIIRS data were based on time series of vegetation indices. However, these indices characterize different aspects of the biophysical properties of vegetation. Indeed, the EVI2 is more sensitive to vegetation gross primary production (GPP), net primary production (NPP), and FPAR (the fraction of photosynthetically active radiation) absorbed by chlorophyll ($FPAR_{chl}$); whereas, the NDVI is more representative of the total leaf variation on a vegetation canopy (including leaves with and without photosynthetic activities) and the FPAR absorbed by the canopy ($FPAR_{canopy}$) (Huete et al., 2013; Zhang et al., 2009a, 2005). Likewise, VCI and GCC also reflect vegetation dynamics differently. VCI emphasizes the green vegetation more strongly as a nonlinear scaling of GCC. In contrast, GCC primarily represents how green the canopy is and only secondarily is sensitive to the amount of foliage, so it could be low for autumn colored foliage even though leaf area index could be still high. As a consequence, it is not surprising that some discrepancies occurred among the phenological dates detected from various datasets. This study demonstrated that EVI2 and NDVI time series were quite similar in detecting spring phenophase transition dates (AADs less than 6 days), while they differed substantially in retrieving senescence phenology (AAD from 10 to 18 days). Although VCI and GCC were very similar in detecting the spring phenology (AAD less than 2 days), they were more different in detecting autumn senescence phenology (AAD being 4–5 days). The different uncertainties in the phenology retrievals between spring and autumn vegetation growing phases likely arise because (1) all of the vegetation indices are constructed to be more sensitive to greens rather than to reds, yellows, or browns, and (2) foliage senescence experiences more gentle transition than the rapid spring flush of new foliage, particularly in forested cover types. Thus, the onset of spring is more readily detected than the onset of autumn.

PhenoCam phenology was more comparable with VIIRS EVI2 phenology than with NDVI phenology in various ecosystems across the CONUS. This finding is consistent with previous results from deciduous forests (Klosterman et al., 2014). Assuming that PhenoCam observations can represent well the phenophase transition dates observed at ground level (Kosmala et al., 2016), it can be concluded that EVI2 is the better choice for detecting phenology than NDVI. Furthermore, EVI2 phenology is closer to VCI than GCC based retrievals, although their differences are smaller than 1 day. Comparing PhenoCam VCI phenology as a proxy for ground observations, we could further conclude that the uncertainty of the VIIRS EVI2 phenology is relatively small for spring phenophase transition dates (7–11 days for the AAD) and large for autumn senescence phenophase transition dates (10–13 days for the AAD). Among all the phenophase transition dates, SOS was best detected, followed by MOS, EOF, EOS, MOF, and SOF.

The difference between VIIRS EVI2 and PhenoCam VCI phenology reveals that VIIRS phenology in forests was well detected with an AAD of 6 days in SOS, followed by grasslands and croplands. However, phenology detection in savannas is complicated, likely due to the spatial heterogeneity captured in the field of view by the PhenoCam and the VIIRS observations. Although the PhenoCam field of view is much larger than other existing ground observations, it is difficult to match well with the actual VIIRS pixel size. Indeed, the spectral reflectances in a 500 m VIIRS pixel represent a median effective resolution of 565 m by 595 m (Campagnolo et al., 2016). As a result, VIIRS phenology detections should be expected to be more comparable to PhenoCam estimates in homogenous sites than in heterogeneous sites. This correspondence was demonstrated in the forest sites where vegetation cover was relatively homogenous, and phenological differences were relatively small, which is in an agreement with the comparison between MODIS phenology and PhenoCam observations in deciduous forests (Klosterman et al., 2014). In contrast, it is challenging to match a VIIRS pixel with a PhenoCam in arid and semiarid savannas where the spatial pattern of vegetation types is highly heterogeneous. This complication was particularly evident at the Tonzi site, California, where grass and tree crown were mixed and phenological dates from PhenoCam in the autumn could differ by more than 3 months between grassland and tree canopy (Liu et al., 2017a). The mixture of different tree and grass proportions leads to large variations in the phenological dates of the savannas. Thus, the VIIRS EVI2 detections were not as consistent with PhenoCam estimates. Because of the difference between PhenoCam and VIIRS imagery, their dissimilarity of phenology detection will increase with the level of heterogeneity or mismatch in the scene. Therefore, the results from this study likely provides the upper boundary of uncertainty in VIIRS phenology detection.

To conduct more accurate evaluations of VIIRS phenology, the mismatch in view geometry and spatial coverage between VIIRS pixels and PhenoCam data could be more fully considered. However, this is very challenging (Baumann et al., 2017; Hufkens et al., 2012; Klosterman et al., 2014; Melaas et al., 2016; Norman et al., 2017; Sonnentag et al., 2012). One solution is to scale up PhenoCam observations to the VIIRS footprint using high temporal and spatial resolution satellite observations (Liu et al., 2017a). The scaling method to bridge accurately between PhenoCam and VIIRS data may become feasible by using the consistent and harmonized surface reflectance product from Landsat-8 OLI (Operational Land Imager) and Sentinel-2 MSI (Multi-Spectral Instrument) data that will be produced from the NASA Harmonized Landsat-Sentinel-2 (HLS) project (https://hls.gsfc.nasa.gov/) (Claverie et al., 2016). However, it should be kept in mind that cloud-free observations in the HLS time series are not always satisfactory for phenology detections and the spatial resolution may be still too coarse to distinguish surface heterogeneity at the Phenocam scale.

To conclude, the results of this study demonstrated that VIIRS LSP metrics are consistent with MODIS LSP and are well characterized and validated using the near-surface remote sensing observations available from the PhenoCam network. With the spatially-distributed dataset of canopy-scale observations from PhenoCam across the CONUS, we have found that VIIRS EVI2 is more suitable for detecting LSP metrics than NDVI and that the overall uncertainty (average absolute difference) on VIIRS LSP phenophase transition dates during entire growing seasons is between 7 and 13 days. The disagreement is less in spring than autumn, less in forests than in croplands or grassland than in savannas, and less in homogenous than in heterogeneous land covers. Consequently, evaluation of VIIRS LSP metrics helps pave the way for more widespread use of VIIRS LSP products and the ability to continue the important MODIS data record.

Acknowledgements

This research was funded in part by NASA projects of Development and Validation of a Global Land Surface Phenology Product from NPP

VIIRS for EOS-MODIS Continuity (NNX15AB96A) and Suomi NPP VIIRS BRDFAlbedo/NBAR Products to Extend the Long Term Consistent Modis Standard Data Record (NNX14AQ18A). ADR acknowledges support for PhenoCam from the Northeastern States Research Cooperative, National Science Foundation's Macrosystems Biology program (awards EF-1065029 and EF-1702697), DOE's Regional and Global Climate Modeling program (award DE-SC0016011), the US National Park Service Inventory and Monitoring Program, and the USA National Phenology Network (grant number G10AP00129 from the United States Geological Survey).

References

Abu-Asab, M.S., Peterson, P.M., Shetler, S.G., Orli, S.S., 2001. Earlier plant flowering in spring as a response to global warming in the Washington, DC, area. Biodivers. Conserv. 10, 597–612.

Atkinson, P.M., Jeganathan, C., Dash, J., Atzberger, C., 2012. Inter-comparison of four models for smoothing satellite sensor time-series data to estimate vegetation phenology. Remote Sens. Environ. 123, 400–417.

Ault, T.R., Schwartz, M.D., Zurita-Milla, R., Weltzin, J.F., Betancourt, J.L., 2015. Trends and natural variability of spring onset in the coterminous United States as evaluated by a new gridded dataset of spring indices. J. Clim. 28, 8363–8378.

Baumann, M., Ozdogan, M., Richardson, A.D., Radeloff, V.C., 2017. Phenology from Landsat when data is scarce: using MODIS and Dynamic Time-Warping to combine multi-year Landsat imagery to derive annual phenology curves. Int. J. Appl. Earth Obs. Geoinf. 54, 72–83.

Bradley, B.A., Jacob, R.W., Hermance, J.F., Mustard, J.F., 2007. A curve fitting procedure to derive inter-annual phenologies from time series of noisy satellite NDVI data. Remote Sens. Environ. 106, 137–145.

Campagnolo, M.L., Sun, Q.S., Liu, Y., Schaaf, C., Wang, Z.S., Roman, M.O., 2016. Estimating the effective spatial resolution of the operational BRDF, albedo, and nadir reflectance products from MODIS and VIIRS. Remote Sens. Environ. 175, 52–64.

Carlson, T.N., Ripley, D.A., 1997. On the relation between NDVI, fractional vegetation cover, and leaf area index. Remote Sens. Environ. 62, 241–252.

Chen, J., Jonsson, P., Tamura, M., Gu, Z.H., Matsushita, B., Eklundh, L., 2004. A simple method for reconstructing a high-quality NDVI time-series data set based on the Savitzky–Golay filter. Remote Sens. Environ. 91, 332–344.

Claverie, M., Masek, J., Ju, J., 2016. Harmonized Landsat-8 Sentinel-2 (HLS) Product User's Guide. https://hls.gsfc.nasa.gov/wp-content/uploads/2017/02/HLS.v1.2.UserGuide.pdf.

Cleland, E.E., Allen, J.M., Crimmins, T.M., Dunne, J.A., Pau, S., Travers, S.E., Zavaleta, E.S., Wolkovich, E.M., 2012. Phenological tracking enables positive species responses to climate change. Ecology 93, 1765–1771.

de Beurs, K.M., Henebry, G.M., 2004. Land surface phenology, climatic variation, and institutional change: analyzing agricultural land cover change in Kazakhstan. Remote Sens. Environ. 89, 497–509.

de Beurs, K.M., Henebry, G.M., 2010. Spatio-temporal statistical methods for modeling land surface phenology. In: Hudson, I.L., Keatley, M.R. (Eds.), Phenological Research – Methods for Environmental and Climate Change Analysis. Spring, New York, pp. 177–208.

de Jong, R., de Bruin, S., de Wit, A., Schaepman, M.E., Dent, D.L., 2011. Analysis of monotonic greening and browning trends from global NDVI time-series. Remote Sens. Environ. 115, 692–702.

Delbart, N., Beaubien, E., Kergoat, L., Toan, T.L., 2015. Comparing land surface phenology with leafing and flowering observations from the PlantWatch citizen network. Remote Sens. Environ. 160, 273–280.

Elmore, A.J., Guinn, S.M., Minsley, B.J., Richardson, A.D., 2012. Landscape controls on the timing of spring, autumn, and growing season length in mid-Atlantic forests. Glob. Change Biol. 18, 656–674.

Friedl, M.A., McIver, D.K., Hodges, J.C.F., Zhang, X.Y., Muchoney, D., Strahler, A.H., Woodcock, C.E., Gopal, S., Schneider, A., Cooper, A., Baccini, A., Gao, F., Schaaf, C., 2002. Global land cover mapping from MODIS: algorithms and early results. Remote Sens. Environ. 83, 287–302.

Friedl, M.A., Sulla-Menashe, D., Tan, B., Schneider, A., Ramankutty, N., Sibley, A., Huang, X.M., 2010. MODIS collection 5 global land cover: algorithm refinements and characterization of new datasets. Remote Sens. Environ. 114, 168–182.

Ganguly, S., Friedl, M.A., Tan, B., Zhang, X.Y., Verma, M., 2010. Land surface phenology from MODIS: characterization of the collection 5 global land cover dynamics product. Remote Sens. Environ. 114, 1805–1816.

Goldberg, M.D., Kilcoyne, H., Cikanek, H., Mehta, A., 2013. Joint Polar Satellite System: The United States next generation civilian polar-orbiting environmental satellite system. J. Geophys. Res. 118, 13463–13475 -Atmospheres.

Golyandina, N., Osipov, E., 2007. The "Caterpillar"-SSA method for analysis of time series with missing data. J. Stat. Plan. Inference 137, 2642–2653.

Henebry, G.M., de Beurs, K.M., 2013. Remote sensing of land surface phenology: a prospectus. In: Schwartz, M.D. (Ed.), Phenology: An Integrative Environmental Science. Springer, pp. 385–411.

Hird, J.N., McDermid, G.J., 2009. Noise reduction of NDVI time series: an empirical comparison of selected techniques. Remote Sens. Environ. 113, 248–258.

Huete, A., Didan, K., Miura, T., Rodriguez, E.P., Gao, X., Ferreira, L.G., 2002. Overview of the radiometric and biophysical performance of the MODIS vegetation indices. Remote Sens. Environ. 83, 195–213.

Huete, A.R., Didan, K., Shimabukuro, Y.E., Ratana, P., Saleska, S.R., Hutyra, L.R., Yang, W.Z., Nemani, R.R., Myneni, R., 2006. Amazon rainforests green-up with sunlight in dry season. Geophys. Res. Lett. 33.

Huete, A., Miura, T., Yoshioka, H., Ratana, P., Broich, M., 2013. Indices of vegetation activity. In: Hanes, J.M. (Ed.), Biophysical Applications of Satellite Remote Sensing. Spring, New York, pp. 1–41.

Hufkens, K., Friedl, M., Sonnentag, O., Braswell, B.H., Milliman, T., Richardson, A.D., 2012. Linking near-surface and satellite remote sensing measurements of deciduous broadleaf forest phenology. Remote Sens. Environ. 117, 307–321.

Ivits, E., Cherlet, M., Toth, G., Sommer, S., Mehl, W., Vogt, J., Micale, F., 2012. Combining satellite derived phenology with climate data for climate change impact assessment. Glob. Planet. Change 88–89, 85–97.

Jiang, Z.Y., Huete, A.R., Didan, K., Miura, T., 2008. Development of a two-band enhanced vegetation index without a blue band. Remote Sens. Environ. 112, 3833–3845.

Jonsson, P., Eklundh, L., 2002. Seasonality extraction by function fitting to time-series of satellite sensor data. IEEE Trans. Geosci. Remote Sens. 40, 1824–1832.

Justice, C.O., Roman, M.O., Csiszar, I., Vermote, E.F., Wolfe, R.E., Hook, S.J., Friedl, M., Wang, Z.S., Schaaf, C.B., Miura, T., Tschudi, M., Riggs, G., Hall, D.K., Lyapustin, A.I., Devadiga, S., Davidson, C., Masuoka, E.J., 2013. Land and cryosphere products from Suomi NPP VIIRS: overview and status. J. Geophys. Res. Atmos. 118, 9753–9765.

Kandasamy, S., Baret, F., Verger, A., Neveux, P., Weiss, M., 2013. A comparison of methods for smoothing and gap filling time series of remote sensing observations—application to MODIS LAI products. Biogeosciences 10, 4055–4071.

Kandasamy, S., Fernandes, R., 2015. An approach for evaluating the impact of gaps and measurement errors on satellite land surface phenology algorithms: application to 20 year NOAA AVHRR data over Canada. Remote Sens. Environ. 164, 114–129.

Keenan, T.F., Richardson, A.D., 2015. The timing of autumn senescence is affected by the timing of spring phenology: implications for predictive models. Glob. Change Biol. 21, 2634–2641.

Klosterman, S.T., Hufkens, K., Gray, J.M., Melaas, E., Sonnentag, O., Lavine, I., Mitchell, L., Norman, R., Friedl, M.A., Richardson, A.D., 2014. Evaluating remote sensing of deciduous forest phenology at multiple spatial scales using PhenoCam imagery. Biogeosciences 11, 4305–4320.

Kosmala, M., Crall, A., Cheng, R., Hufkens, K., Henderson, S., Richardson, A.D., 2016. Season spotter: using citizen science to validate and scale plant phenology from near-surface remote sensing. Remote Sens. 8, 726.

Liang, L.A., Schwartz, M.D., Fei, S.L., 2011. Validating satellite phenology through intensive ground observation and landscape scaling in a mixed seasonal forest. Remote Sens. Environ. 115, 143–157.

Liang, L., Schwartz, M.D., Wang, Z.S., Gao, F., Schaaf, C.B., Tan, B., Morisette, J.T., Zhang, X.Y., 2014. A cross comparison of spatiotemporally enhanced springtime phenological measurements from satellites and ground in a Northern U.S. mixed forest. IEEE Trans. Geosci. Remote Sens. 52, 7513–7526.

Liu, Y., Hill, M.J., Zhang, X., Wang, Z., Richardson, A.D., Hufkens, K., Filippa, G., Baldocchi, D.D., Ma, S., Verfaillie, J., Schaaf, C.B., 2017a. Using data from Landsat, MODIS, VIIRS and PhenoCams to monitor the phenology of California oak/grass savanna and open grassland across spatial scales. Agric. For. Meteorol. 237, 311–325.

Liu, Y., Wang, Z., Sun, Q., Erb, A.M., Schaaf, C.B., Zhang, X., Román, M.O., Scott, R.L., Zhang, Q., Novick, K.A., Bret-Harte, M.S., Petroy, S., SanClements, M., 2017b. Evaluation of the VIIRS BRDF, Albedo and NBAR products 1 and an assessment of continuity with the long term MODIS record. Remote Sens. Environ. 201, 256–274.

Melaas, E.K., Friedl, M.A., Zhu, Z., 2013. Detecting interannual variation in deciduous broadleaf forest phenology using landsat TM/ETM plus data. Remote Sens. Environ. 132, 176–185.

Melaas, E.K., Sulla-Menashe, D., Gray, J.M., Black, T.A., Morin, T.H., Richardson, A.D., Friedl, M.A., 2016. Multisite analysis of land surface phenology in North American temperate and boreal deciduous forests from Landsat. Remote Sens. Environ. 186, 452–464.

Menzel, A., Sparks, T.H., Estrella, N., Roy, D.B., 2006. Altered geographic and temporal variability in phenology in response to climate change. Glob. Ecol. Biogeogr. 15, 498–504.

Moody, A., Johnson, D.M., 2001. Land-surface phenologies from AVHRR using the discrete fourier transform. Remote Sens. Environ. 75, 305–323.

Morin, X., Lechowicz, M.J., Augspurger, C., O'Keefe, J., Viner, D., Chuine, I., 2009. Leaf phenology in 22 North American tree species during the 21st century. Glob. Change Biol. 15, 961–975.

Morisette, J.T., Richardson, A.D., Knapp, A.K., Fisher, J.I., Graham, E.A., Abatzoglou, J., Wilson, B.E., Breshears, D.D., Henebry, G.M., Hanes, J.M., Liang, L., 2009. Tracking the rhythm of the seasons in the face of global change: phenological research in the 21st century. Front. Ecol. Environ. 7, 253–260.

Myneni, R.B., Keeling, C.D., Tucker, C.J., Asrar, G., Nemani, R.R., 1997. Increased plant growth in the northern high latitudes from 1981 to 1991. Nature 386, 698–702.

Myneni, R.B., Hoffman, S., Knyazikhin, Y., Privette, J.L., Glassy, J., Tian, Y., Wang, Y., Song, X., Zhang, Y., Smith, G.R., Lotsch, A., Friedl, M., Morisette, J.T., Votava, P., Nemani, R.R., Running, S.W., 2002. Global products of vegetation leaf area and fraction absorbed PAR from year one of MODIS data. Remote Sens. Environ. 83, 214–231.

Norman, S.P., Hargrove, W., Christie, W.M., 2017. Spring and autumn phenological variability across environmental gradients of Great Smoky Mountains National Park, USA. Remote Sens. 9.

Parmesan, C., Yohe, G., 2003. A globally coherent fingerprint of climate change impacts across natural systems. Nature 421, 37–42.

Reed, B.C., Brown, J.F., VanderZee, D., Loveland, T.R., Merchant, J.W., Ohlen, D.O., 1994. Measuring phenological variability from satellite imagery. J. Veg. Sci. 5, 703–714.

Ratkowsky, D.A., 1983. Nonlinear Regression Modeling—A Unified Practical Approach.

Marcel Dekker, New York and Basel.
Richards, F.J., 1959. A flexible growth function for empirical use. J. Exp. Bot. 10, 290–300.
Richardson, A.D., Bailey, A.S., Denny, E.G., Martin, C.W., O'Keefe, J., 2006. Phenology of a northern hardwood forest canopy. Glob. Change Biol. 12, 1174–1188.
Richardson, A.D., Jenkins, J.P., Braswell, B.H., Hollinger, D.Y., Ollinger, S.V., Smith, M.L., 2007. Use of digital webcam images to track spring green-up in a deciduous broadleaf forest. Oecologia 152, 323–334.
Richardson, A.D., Braswell, B.H., Hollinger, D.Y., Jenkins, J.P., Ollinger, S.V., 2009a. Near-surface remote sensing of spatial and temporal variation in canopy phenology. Ecol. Appl. 19, 1417–1428.
Richardson, A.D., Hollinger, D.Y., Dail, D.B., Lee, J.T., Munger, J.W., O'Keefe, J., 2009b. Influence of spring phenology on seasonal and annual carbon balance in two contrasting New England forests. Tree Physiol. 29, 321–331.
Rodriguez-Galiano, V.F., Dash, J., Atkinson, P.M., 2015. Intercomparison of satellite sensor land surface phenology and ground phenology in Europe. Geophys. Res. Lett. 42, 2253–2260.
Roman, M.O., Gatebe, C.K., Schaaf, C.B., Poudyal, R., Wang, Z.S., King, M.D., 2011. Variability in surface BRDF at different spatial scales (30 m–500 m) over a mixed agricultural landscape as retrieved from airborne and satellite spectral measurements. Remote Sens. Environ. 115, 2184–2203.
Sakamoto, T., Wardlow, B.D., Gitelson, A.A., Verma, S.B., Suyker, A.E., Arkebauer, T.J., 2010. A two-step filtering approach for detecting maize and soybean phenology with time-series MODIS data. Remote Sens. Environ. 114, 2146–2159.
Schaaf, C.B., Gao, F., Strahler, A.H., Lucht, W., Li, X.W., Tsang, T., Strugnell, N.C., Zhang, X.Y., Jin, Y.F., Muller, J.P., Lewis, P., Barnsley, M., Hobson, P., Disney, M., Roberts, G., Dunderdale, M., Doll, C., d'Entremont, R.P., Hu, B.X., Liang, S.L., Privette, J.L., Roy, D., 2002. First operational BRDF, albedo nadir reflectance products from MODIS. Remote Sens. Environ. 83, 135–148.
Schaaf, C.B., Liu, J., Gao, F., Strahler, A.H., 2011. MODIS albedo and reflectance an isotropy products from Aqua and Terra. In: Ramachandran, B., Justice, C., Abrams, M. (Eds.), Land Remote Sensing and Global Environmental Change: NASA's Earth Observing System and the Science of ASTER and MODIS. Springer-Cerlag, pp. 549–562.
Schaber, J., Badeck, F.W., 2003. Physiology-based phenology models for forest tree species in Germany. Int. J. Biometeorol. 47, 193–201.
Schwartz, M.D., 1999. Advancing to full bloom: planning phenological research for the 21st century. Int. J. Biometeorol. 42, 113–118.
Schwartz, M.D., Reed, B.C., White, M.A., 2002. Assessing satellite-derived start-of-season measures in the conterminous USA. Int. J. Climatol. 22, 1793–1805.
Schwartz, M.D., Ahas, R., Aasa, A., 2006. Onset of spring starting earlier across the Northern Hemisphere. Glob. Change Biol. 12, 343–351.
Schwartz, M.D., Ault, T.R., Betancourt, J.L., 2013. Spring onset variations and trends in the continental United States: past and regional assessment using temperature-based indices. Int. J. Climatol. 33, 2917–2922.
Sonnentag, O., Hufkens, K., Teshera-Sterne, C., Young, A.M., Friedl, M., Braswell, B.H., Milliman, T., O'Keefe, J., Richardson, A.D., 2012. Digital repeat photography for phenological research in forest ecosystems. Agric. For. Meteorol. 152, 159–177.
Soudani, K., le Maire, G., Dufrene, E., Francois, C., Delpierre, N., Ulrich, E., Cecchini, S., 2008. Evaluation of the onset of green-up in temperate deciduous broadleaf forests derived from moderate resolution imaging spectroradiometer (MODIS) data. Remote Sens. Environ. 112, 2643–2655.
Tan, B., Morisette, J.T., Wolfe, R.E., Gao, F., Ederer, G.A., Nightingale, J., Pedelty, J.A., 2011. An enhanced TIMESAT algorithm for estimating vegetation phenology metrics from MODIS data. IEEE J. Sel. Top. Appl. Earth Obs. Remote Sens. 4, 361–371.
Toomey, M., Friedl, M.A., Frolking, S., Hufkens, K., Klosterman, S., Sonnentag, O., Baldocchi, D.D., Bernacchi, C.J., Biraud, S.C., Bohrer, G., Brzostek, E., Burns, S.P., Coursolle, C., Hollinger, D.Y., Margolis, H.A., McCaughey, H., Monson, R.K., Munger, J.W., Pallardy, S., Phillips, R.P., Torn, M.S., Wharton, S., Zeri, M., Richardson, A.D., 2015. Greenness indices from digital cameras predict the timing and seasonal dynamics of canopy-scale photosynthesis. Ecol. Appl. 25, 99–115.
Verger, A., Baret, F., Weiss, M., 2011. A multisensor fusion approach to improve LAI time series. Remote Sens. Environ. 115, 2460–2470.
Verger, A., Baret, F., Weiss, M., Kandasamy, S., Vermote, E., 2013. The CACAO method for smoothing, gap filling, and characterizing seasonal anomalies in satellite time series. IEEE Trans. Geosci. Remote Sens. 51, 1963–1972.
Vina, A., Tuanmu, M.N., Xu, W.H., Li, Y., Qi, J.G., Ouyang, Z.Y., Liu, J.G., 2012. Relationship between floristic similarity and vegetated land surface phenology: Implications for the synoptic monitoring of species diversity at broad geographic regions. Remote Sens. Environ. 121, 488–496.
Wang, Z.S., Schaaf, C.B., Chopping, M.J., Strahler, A.H., Wang, J.D., Roman, M.O., Rocha, A.V., Woodcock, C.E., Shuai, Y.M., 2012. Evaluation of moderate-resolution imaging spectroradiometer (MODIS) snow albedo product (MCD43A) over tundra. Remote Sens. Environ. 117, 264–280.
White, M.A., Nemani, R.R., 2006. Real-time monitoring and short-term forecasting of land surface phenology. Remote Sens. Environ. 104, 43–49.
White, M.A., Thornton, P.E., Running, S.W., 1997. A continental phenology model for monitoring vegetation responses to interannual climatic variability. Glob. Biogeochem. Cycl. 11, 217–234.
White, M.A., de Beurs, K.M., Didan, K., Inouye, D.W., Richardson, A.D., Jensen, O.P., O'Keefe, J., Zhang, G., Nemani, R.R., van Leeuwen, W.J.D., Brown, J.F., de Wit, A., Schaepman, M., Lin, X.M., Dettinger, M., Bailey, A.S., Kimball, J., Schwartz, M.D., Baldocchi, D.D., Lee, J.T., Lauenroth, W.K., 2009. Intercomparison, interpretation, and assessment of spring phenology in North America estimated from remote sensing for 1982–2006. Glob. Change Biol. 15, 2335–2359.
Wingate, L., Ogee, J., Cremonese, E., Filippa, G., Mizunuma, T., Migliavacca, M., Moisy, C., Wilkinson, M., Moureaux, C., Wohlfahrt, G., Hammerle, A., Hortnagl, L., Gimeno, C., Porcar-Castell, A., Galvagno, M., Nakaji, T., Morison, J., Kolle, O., Knohl, A., Kutsch, W., Kolari, P., Nikinmaa, E., Ibrom, A., Gielen, B., Eugster, W., Balzarolo, M., Papale, D., Klumpp, K., Kostner, B., Grunwald, T., Joffre, R., Ourcival, J.M., Hellstrom, M., Lindroth, A., George, C., Longdoz, B., Genty, B., Levula, J., Heinesch, B., Sprintsin, M., Yakir, D., Manise, T., Guyon, D., Ahrends, H., Plaza-Aguilar, A., Guan, J.H., Grace, J., 2015. Interpreting canopy development and physiology using a European phenology camera network at flux sites. Biogeosciences 12, 5995–6015.
Xiao, W.W., Sun, Z.G., Wang, Q.X., Yang, Y.H., 2013. Evaluating MODIS phenology product for rotating croplands through ground observations. J. Appl. Remote Sens. 7.
Zhang, X.Y., 2015. Reconstruction of a complete global time series of daily vegetation index trajectory from long-term AVHRR data. Remote Sens. Environ. 156, 457–472.
Zhang, X.Y., Friedl, M.A., Schaaf, C.B., Strahler, A.H., Hodges, J.C.F., Gao, F., Reed, B.C., Huete, A., 2003. Monitoring vegetation phenology using MODIS. Remote Sens. Environ. 84, 471–475.
Zhang, Q.Y., Xiao, X.M., Braswell, B., Linder, E., Baret, F., Moore, B., 2005. Estimating light absorption by chlorophyll, leaf and canopy in a deciduous broadleaf forest using MODIS data and a radiative transfer model. Remote Sens. Environ. 99, 357–371.
Zhang, X.Y., Friedl, M.A., Schaaf, C.B., 2006. Global vegetation phenology from moderate resolution imaging spectroradiometer (MODIS): evaluation of global patterns and comparison with in situ measurements. J. Geophys. Res.—Biogeosci. 111.
Zhang, X.Y., Tarpley, D., Sullivan, J.T., 2007. Diverse responses of vegetation phenology to a warming climate. Geophys. Res. Lett. 34.
Zhang, Q.Y., Middleton, E.M., Margolis, H.A., Drolet, G.G., Barr, A.A., Black, T.A., 2009a. Can a satellite-derived estimate of the fraction of PAR absorbed by chlorophyll (FAPAR(chl)) improve predictions of light-use efficiency and ecosystem photosynthesis for a boreal aspen forest? Remote Sens. Environ. 113, 880–888.
Zhang, X., Friedl, M., Schaaf, C., 2009b. Sensitivity of vegetation phenology detection to the temporal resolution of satellite data. Int. J. Remote Sens. 30, 2061–2074.
Zhang, X.Y., Goldberg, M.D., Yu, Y.Y., 2012. Prototype for monitoring and forecasting fall foliage coloration in real time from satellite data. Agric. For. Meteorol. 158, 21–29.
Zhang, X.Y., Tan, B., Yu, Y.Y., 2014. Interannual variations and trends in global land surface phenology derived from enhanced vegetation index during 1982–2010. Int. J. Biometeorol. 58, 547–564.
Zhang, X.Y., Liu, L.L., Yan, D., 2017. Comparisons of global land surface seasonality and phenology derived from AVHRR, MODIS, and VIIRS data. J. Geophys. Res.—Biogeosci. 122, 1506–1525.